
DCT-Based Decorrelated Attention for Vision Transformers

Hongyi Pan^{*†}, Emadeldeen Hamdan[‡], Xin Zhu[‡], Koushik Biswas[†], Ahmet Enis Cetin[‡], Ulas Bagci[†]

[†]Machine and Hybrid Intelligence Lab, Northwestern University, Chicago, IL 60611

[‡]Department of Electrical and Computer Engineering, University of Illinois Chicago Chicago, IL 60607

^{*}hongyi.pan@northwestern.edu

Abstract

Central to the *Transformer architectures*' effectiveness is the self-attention mechanism, a function that maps queries, keys, and values into a high-dimensional vector space. However, training the attention weights of queries, keys, and values is non-trivial from a state of random initialization. In this paper, we propose two methods. (i) We first address the initialization problem of Vision Transformers by introducing a simple, yet highly innovative, initialization approach utilizing Discrete Cosine Transform (DCT) coefficients. Our proposed DCT-based *attention* initialization marks a significant gain compared to traditional initialization strategies; offering a robust foundation for the attention mechanism. Our experiments reveal that the DCT-based initialization enhances the accuracy of Vision Transformers in classification tasks. (ii) We also recognize that since DCT effectively decorrelates image information in the frequency domain, this decorrelation is useful for compression because it allows the quantization step to discard many of the higher-frequency components. Based on this observation, we propose a novel DCT-based compression technique for the attention function of Vision Transformers. Since high-frequency DCT coefficients usually correspond to noise, we truncate the high-frequency DCT components of the input patches. Our DCT-based compression reduces the size of weight matrices for queries, keys, and values. While maintaining the same level of accuracy, our DCT compressed Swin Transformers obtain a considerable decrease in the computational overhead.

1 Introduction

In the last decade, convolutional neural networks (CNNs) have dominated image-processing tasks. However, inspired by the success of transformer architectures in natural language processing, Vision Transformers (ViTs) in recent years have redefined the norms of visual data interpretation. Self-attention mechanism, a key component of transformers, is pivotal in reshaping how models perceive and analyze visual information [49]. Unlike CNNs, ViTs view an image as a sequence of informative patches, adopting a more holistic approach. By treating image patches like “visual words”, ViTs can leverage powerful transformer architectures, originally designed for natural language processing, to learn global context and long-range dependencies. This novel approach has led to remarkable performance gains on a wide range of computer vision tasks, demonstrating the potential of ViTs to revolutionize the field.

The initialization of self-attention weights is a critical step significantly impacting the training dynamics and performance of the Transformers. The core of Transformers is the *self-attention* mechanism, which includes three weight matrices: queries (\mathbf{W}_Q), keys (\mathbf{W}_K), and values (\mathbf{W}_V). Proper initialization of these matrices ensures that the model starts from a stable state, facilitating effective learning. The most common approach is to initialize the weights randomly, often using

distributions like the normal or uniform distribution. For example, Xavier initialization [16] and He initialization [18] are popular choices. They are designed to keep the scale of the gradients roughly the same in all layers. Although less common, in some cases, biases or certain parts of the weight matrices are initialized to zeros [32, 60]. This is less common for queries, keys, and values matrices, as it can lead to symmetry-breaking issues during training [20].

Efficiency is an ongoing concern in Transformers. While conventional initialization strategies are often suitable for generic applications, new algorithms are increasingly tailored to the specific characteristics and needs of Transformers. These advancements in initialization techniques contribute to the ongoing improvements in the performance and efficiency of Transformer-based models. Orthogonal initialization [40, 21], sparse initialization [31], variance scaling, pre-trained initialization [51, 4], layer-wise, domain-specific and attention-specific initialization [48] are some of the new trends in initialization approaches. In this study, we propose a new family of algorithms for initialization strategy in the intersection of attention and domain-specific approaches: *discrete cosine attention*.

Can DCT in Vision Transformer be a game changer? Discrete cosine transform (DCT) has been widely used in signal processing and data compression applications. It reduces the dimensionality of the input data while preserving its essential features. Transforming the input data into the frequency domain helps capture the most important features of the input data. In this paper, we propose two methods that apply DCT to the attention for vision transformers. First, we initialize the weight matrices for the queries, keys, and values computation as the DCT matrix. Our DCT-based initialization covers the entire spectrum utilizing the DCT basis vectors, and each weight vector has a different initial bandwidth. As a comparison, to cover the entire spectrum in the classical initialization, all the weight matrices are initialized as random numbers due to their independent generation. These random numbers can be treated as white noise. All the weight initialization starts with the same spectra. Second, we introduce a DCT-based compressed attention for vision transformers. With this compression methodology, compared to the vanilla Swin transformers, the number of parameters and computational overhead of the Swin Transformers are reduced. Meanwhile, the accuracy of the models is comparable.

2 Related works

Vision Transformers Transformer architectures have merged as a dominant standard for natural language processing (NLP) tasks [49, 53]. Vision Transformer (ViT) [14] built a bridge between language and vision. It shows that pure transformers can also be applied directly to sequences of image patches for classification tasks. In other words, it partitions images into patches and treats them as word sequences. Then, a shifted windowing scheme was proposed in Swin Transformer [29] to obtain greater efficiency. This limits self-attention computation to non-overlapping local windows while allowing for cross-window connection. Later, to overcome the limitations of the heavyweights in ViTs, MobileViT [33] combined the strengths of MobileNets [39] and ViTs. It is a lightweight and low-latency network for mobile vision tasks. Moreover, gSwin [17] combined MLP-based architecture with Swin Transformer and attains superior accuracy with a smaller model size. Vision transformers are now supreme in various computer vision tasks such as super resolution [27, 57], compressive sensing [43, 54], image segmentation [59, 23, 47], and human mesh reconstruction [62].

Frequency-based Neural Networks Orthogonal transforms such as Fourier transform [10, 5], Hadamard transform [34, 36], and discrete cosine Stockwell transform [64] have been used to improve the performance of the neural networks. In the orthogonal transform family, DCT is a mathematical technique commonly used in signal processing and image and video compression [35]. Compared to the Fourier transform, which is the standard frequency representation, DCT does not generate complex-valued numbers. Therefore, it is computationally more efficient. DCT-Former [41], for instance, applied DCT compression on the input sequence along the length channel before feeding into the self-attention layers to reduce the computational overhead in the NLP problems. Furthermore, inspired by JPEG compression, DCFormer [26] highlighted the visually significant signals by leveraging the input information compression on its frequency domain representation. These two DCT-based works and our DCT-based compression all aim to reduce the computational overhead. Therefore, we mainly compare our DCT-based compression method with them. DCT-Former [41] is designed for the NLP transformers and takes DCT along the width and height of the input tensor patches, while our method is designed for the vision transformers and it compresses the tensor along the channel axis. DCFormer [26] averages DCT coefficients via average pooling,

which does not take advantage of the property that DCT components in low-frequency contain more important information. On the contrary, our DCT-based compression method retains the low-frequency components very accurately and discards the unnecessary extremely high-frequency components corresponding to noise. Under the same input image size, compared to the vanilla transformer models, DCFormer reduces the FLOPs and retains the number of parameters while sacrificing accuracy. Our DCT-based compression method, on the other hand, saves both trainable parameters and FLOPs and obtains on-par or better performance in addition to other benefits that our DCT-based compression method has. Furthermore, we introduce a DCT-based initialization and we have not found any related initialization in the literature.

Initialization Methods for Self-Attention Mimetic initialization [48] is a compute-free method to initialize the weights of self-attention layers. It simulated the patterns present in the pre-trained weights to achieve performance improvement of the transformers.

Efficient Multi-head Self-Attention To reduce the memory and computational costs of dot-product attention, an efficient mechanism [42] in linear complexity was proposed. Besides, Hydra Attention [3] increased the number of heads to address the issue of the high computational complexity of the self-attention mechanism on large-sized images. Further, MetaFormer [55] verified that the overall architecture of Transformers, rather than the specific token mixer module, plays a more crucial role in the performance.

3 Methodology

3.1 Background: Multi-Head Self-Attention

The overall structure of the vanilla MSA is drawn in Figure 1a. To handle a 2D image tensor $\mathbf{I} \in \mathbb{R}^{H \times W \times C}$, where $H \times W$ are the resolution of the image and C is the number of channels, we first split it into patches $\mathbf{X} \in \mathbb{R}^{N \times M^2 \times C}$, where $M \times M$ is the resolution of each image patch and $N = \frac{WH}{M^2}$ is the resulting number of patches. After that, three linear layers ($\mathcal{L}_Q, \mathcal{L}_K, \mathcal{L}_V$) are applied on \mathbf{X} to compute the queries, keys, and values $\mathbf{Q}, \mathbf{K}, \mathbf{V} \in \mathbb{R}^{N \times M^2 \times C}$:

$$\mathbf{Q} = \mathbf{X}\mathbf{W}_Q^T + \mathbf{b}_Q, \quad \mathbf{K} = \mathbf{X}\mathbf{W}_K^T + \mathbf{b}_K, \quad \mathbf{V} = \mathbf{X}\mathbf{W}_V^T + \mathbf{b}_V, \quad (1)$$

where $\mathbf{W}_Q, \mathbf{W}_K, \mathbf{W}_V \in \mathbb{R}^{C \times C}$ and $\mathbf{b}_Q, \mathbf{b}_K, \mathbf{b}_V \in \mathbb{R}^{1 \times C}$ are trainable weights and biases. Next, to perform multi-head attention with P heads, $\mathbf{Q}, \mathbf{K}, \mathbf{V}$ are split into P slices as $\mathbf{Q}_i, \mathbf{K}_i, \mathbf{V}_i \in \mathbb{R}^{N \times M^2 \times d}$ for $i = 0, \dots, P-1$, where $d = \frac{C}{P}$. The scaled dot-product attention $\mathbf{A}_i \in \mathbb{R}^{N \times M^2 \times d}$ is computed as:

$$\mathbf{A}_i = \text{Attention}(\mathbf{Q}_i, \mathbf{K}_i, \mathbf{V}_i) = \sigma \left(\frac{\mathbf{Q}_i \mathbf{K}_i^T}{\sqrt{d}} + \mathbf{B}_i \right) \mathbf{V}_i, \quad (2)$$

where $\sigma(\cdot)$ is the *Softmax* function. $\mathbf{B}_i \in \mathbb{R}^{M^2 \times M^2}$ is the relative position bias. Since the relative position along each axis lies in $[-M+1, M-1]$, values in \mathbf{B}_i are taken from a parameterized smaller-sized bias matrix $\hat{\mathbf{B}}_i \in \mathbb{R}^{(2M-1) \times (2M-1)}$. After that, $\{\mathbf{A}_i\}$ are concatenated to $\mathbf{A} \in \mathbb{R}^{N \times M^2 \times C}$ to feed into a linear layer \mathcal{L}_O to obtain the attention output $\mathbf{Y} \in \mathbb{R}^{N \times M^2 \times C}$:

$$\mathbf{Y} = \mathbf{A}\mathbf{W}_O^T + \mathbf{b}_O. \quad (3)$$

Finally, \mathbf{Y} is reversed into the image shape $\mathbf{J} \in \mathbb{R}^{H \times W \times C}$.

3.2 DCT-based Initialization for Attention

In the attention layer, the first three linear layers ($\mathcal{L}_Q, \mathcal{L}_K$, and \mathcal{L}_V) extract different features of the input patches \mathbf{X} . However, their weights $\mathbf{W}_Q, \mathbf{W}_K$, and \mathbf{W}_V are trained simultaneously. Such training from scratch is difficult, especially when the dataset is insufficient and small-scale. On the other hand, DCT is a well-designed feature extractor. In our proposed DCT initialization strategy, one of $\mathbf{W}_Q, \mathbf{W}_K, \mathbf{W}_V \in \mathbb{R}^{C \times C}$ is initialized using the orthogonal type-II DCT matrix \mathcal{D} [1]:

$$\{\mathbf{X}\mathcal{D}^T\}[k] = \begin{cases} \frac{\sqrt{2}}{C} \sum_{n=0}^{C-1} \mathbf{X}[n], & k = 0, \\ \frac{2}{C} \sum_{n=0}^{C-1} \mathbf{X}[n] \cos \frac{(2n+1)k\pi}{2nC}, & k = 1, \dots, C-1. \end{cases} \quad (4)$$

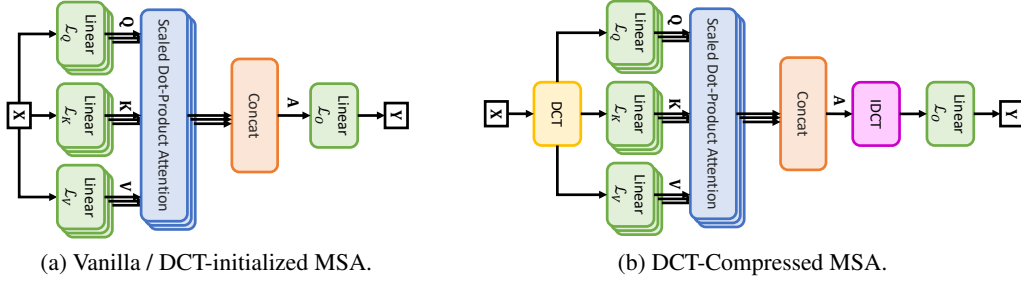


Figure 1: Multi-head Self-Attention. In (b), to reduce the computational overhead, IDCT and the final linear layer \mathcal{L}_O are implemented as a single linear layer as no non-linearity exists in between.

D can be obtained from applying DCT on an identity matrix $\mathbf{I}_{C \times C}$ because DCT is a linear transform. The remaining weight matrices and other trainable parameters are still initialized regularly. We don't initialize multiple weight matrices to avoid the weight symmetry problem [20] caused by initializing the multiple weights as the same values, and our ablation study has verified this point.

The DCT-based initialization can be treated as applying DCT instead of linear projection on \mathbf{X} to obtain \mathbf{Q} , \mathbf{K} , or \mathbf{V} . Some DCT coefficients capture low-frequency information, while others capture high-frequency details. Therefore, the DCT matrix is a good starting point for the weight matrices.

3.3 DCT-Based Compressed Attention

Data compression using DCT is common in signal, image, and video processing for energy concentration, compression efficiency, and noise reduction. DCT not only decorrelates the input image data similar to the Karhunen-Loeve Transform (KLT) or principal component analysis (PCA) but also has a frequency interpretation because it can be computed using the discrete Fourier transform (DFT) [1]:

$$\{\mathbf{X}D^T\}[k] = \begin{cases} \frac{\sqrt{2}}{C} \sum_{n=0}^{C-1} \mathbf{X}[n], & k = 0, \\ \frac{2}{C} \text{Re} \left(e^{-\frac{ik\pi}{2C}} \sum_{n=0}^{2C-1} \mathbf{X}[n]W^{kn} \right), & k = 1, \dots, C-1, \end{cases} \quad (5)$$

where $W = e^{-\frac{i2\pi}{2C}}$, $i^2 = -1$, and $\text{Re}(\cdot)$ implies the real part of the term enclosed. Usually, higher-frequency DCT coefficients contribute less to perceptual quality and contain more noise. Therefore, preserving essential information in lower frequencies while discarding less critical details in higher frequencies results in efficient signal representation and storage. The specific truncation strategy depends on the application's requirements and the acceptable level of information loss.

We observed that the attention layer matrices are correlated with each other so that we can compress them using DCT. Figure 1b shows the method of DCT-based compression for the attention layer. First, the input patches $\mathbf{X} \in \mathbb{R}^{N \times M^2 \times C}$ are encoded by DCT along the channel of C with the high-frequency components truncated. If we keep the first τC coefficients ($\tau < 1$), the essential information of \mathbf{X} is still preserved, while the input and output dimensions of the linear layers (\mathcal{L}_Q , \mathcal{L}_K , and \mathcal{L}_V) are reduced from $\mathbb{R}^{N \times M^2 \times C}$ to $\mathbb{R}^{N \times M^2 \times \tau C}$. In this way, the computational cost from \mathcal{L}_Q , \mathcal{L}_K , and \mathcal{L}_V is reduced significantly. In our experiments, τ is chosen from 25%, 50%, and 75%. After obtaining the attention $\mathbf{A} \in \mathbb{R}^{N \times M^2 \times \tau C}$ from the queries \mathbf{Q} , keys \mathbf{K} , and values \mathbf{V} , we apply zero-padding along the last channel to make the dimension back to $\mathbb{R}^{N \times M^2 \times C}$. Before being fed into the linear layer \mathcal{L}_O , these padded patches are decoded by the inverse DCT (IDCT):

$$\{\mathbf{A}(D^{-1})^T\}[n] = \frac{\sqrt{2}}{2} \mathbf{A}[0] + \sum_{k=1}^{C-1} \mathbf{A}[k] \cos \frac{(2n+1)k\pi}{2C}, n = 0, 1, \dots, C-1. \quad (6)$$

DCT and IDCT can be implemented in a fast manner with the complexity of $O(C \log_2 C)$ using butterfly algorithm [9]. However, such an implementation is not officially supported in PyTorch currently. Therefore, in this work, we implement the DCT and IDCT via matrix multiplication between the input tensor and the truncated DCT and IDCT matrices $\tilde{D} \in \mathbb{R}^{\tau C \times C}$ and $\tilde{D}^{-1} \in \mathbb{R}^{C \times \tau C}$. These transform matrices are obtained by truncating the DCT and IDCT matrices along rows or columns to keep τ coefficients or zero padding, respectively. Then, DCT with truncation or IDCT with

Table 1: Multiplications in MSA on $\mathbf{X} \in \mathbb{R}^{N \times M^2 \times C}$. “-” means this step is not required. $\tau < 1$.

Operation	Vanilla MSA	DCT-Compressed MSA	
		Naive	Simplified
DCT	-	$\tau NM^2 C^3$	$\tau NM^2 C^3$
$\mathcal{L}_Q, \mathcal{L}_K, \mathcal{L}_V$	$3NM^2 C^3$	$3\tau^2 NM^2 C^3$	$3\tau^2 NM^2 C^3$
$\mathbf{Q}\mathbf{K}^T/\sqrt{d} + \mathbf{B}$	$NM^4 C^2$	$\tau^2 NM^4 C^2$	$\tau^2 NM^4 C^2$
Multiply with \mathbf{V}	$NM^4 C^2$	$\tau^2 NM^4 C^2$	$\tau^2 NM^4 C^2$
IDCT	-	$\tau NM^2 C^3$	-
\mathcal{L}_O	$NM^2 C^3$	$NM^2 C^3$	$\tau NM^2 C^3$
Total	$4NM^2 C^3$ $+2NM^4 C^2$	$(1 + 2\tau + 3\tau^2)NM^2 C^3$ $+2\tau^2 NM^4 C^2$	$(2\tau + 3\tau^2)NM^2 C^3$ $+2\tau^2 NM^4 C^2$

zero padding is implemented as one matrix multiplication to reduce memory pressure. Furthermore, as no non-linearity exists between IDCT and the final linear layer \mathcal{L}_O , these two steps can be implemented as a single linear layer whose weight matrix is $\mathbf{W}_O \bar{\mathbf{D}}^{-1}$ and the bias is still \mathbf{b}_O . However, such a combination is not applied on DCT and \mathbf{W}_Q , \mathbf{W}_K , or \mathbf{W}_V . This is because it may not always reduce the computational cost for them: To compute \mathbf{Q} , \mathbf{K} , and \mathbf{V} , with such a combination, $3kNM^2 C^3$ multiplications are needed. In contrast, if they are computed separately, there are $\tau NM^2 C^3$ multiplications from DCT and $\tau^2 NM^2 C^3$ multiplications from each linear layer. As a result, there are a total of $(\tau + 3\tau^2)NM^2 C^3$ multiplications. Hence, combing DCT with \mathbf{W}_Q , \mathbf{W}_K and \mathbf{W}_V brings computational cost saving only when $\tau > \frac{2}{3}$. To maintain the consistency of the framework, we do not combine DCT with \mathbf{W}_Q , \mathbf{W}_K , or \mathbf{W}_V .

Computational cost comparison of the vanilla versus the proposed DCT-compressed attentions is presented in Table 1. We evaluate both naive and simplified implementations of the DCT-compressed attention with the vanilla attention. The simplification is implemented by fusing IDCT into the linear layer \mathcal{L}_O . Computational overhead from the Softmax function is omitted because the Softmax function is based on exponential terms. Despite this, the Softmax function in the DCT-compressed attention requires less computational cost than in the vanilla attention as the number of entries in $\left(\frac{\mathbf{Q}\mathbf{K}^T}{\sqrt{d}} + \mathbf{B}\right)$ in the DCT-compressed attention is τ^2 times ($\tau < 1$) as in the vanilla attention.

3.4 Frequency Domain Motivation of the DCT-based Initialization

In traditional random initialization, all the weight matrices are initialized as random numbers that are independently generated. As a result, the initial matrices can be considered as a realization of white noise covering the entire spectrum. A good initialization should take advantage of the full bandwidth to cover the entire spectrum of the input.

The DCT-based initialization also covers the entire frequency domain. The set of DCT basis vectors $\left\{\frac{\sqrt{2}}{2}, \cos\left(\frac{(2n+1)k\pi}{2C}\right)\right\}$ is the class of discrete Chebyshev polynomials:

$$T_k[n] = \begin{cases} \frac{\sqrt{2}}{2}, & k = 0, \\ \cos\left(\frac{(2n+1)k\pi}{2C}\right), & k = 1, \dots, C-1, \end{cases} \quad (7)$$

for $n = 0, 1, \dots, C-1$. The basis member $\cos\left(\frac{(2n+1)k\pi}{2C}\right)$ is the k -th Chebyshev polynomial $T_k[\xi]$ evaluated at the n -th zero of $T_n[\xi]$ [1]. Figure 2 draws the basis vectors in Eq. (7) for an 8×8 DCT matrix and the magnitude of their discrete Fourier transform ($\mathcal{F}\{\cdot\}$):

$$\hat{T}_l[k] = \mathcal{F}\{T_l[n]\}, l = 0, 1, \dots, C-1. \quad (8)$$

Therefore, the entire spectrum is covered as $\sqrt{\sum_{l=0}^{C-1} |\hat{T}_l[k]|^2}$ has perfect full-band coverage, and each weight vector in the DCT-based initialization covers a different bandwidth. On the other hand, in the traditional random initialization, all of the weights start with the same spectra. This is why our DCT-based initialization is superior to the traditional random initialization for the attention layer.

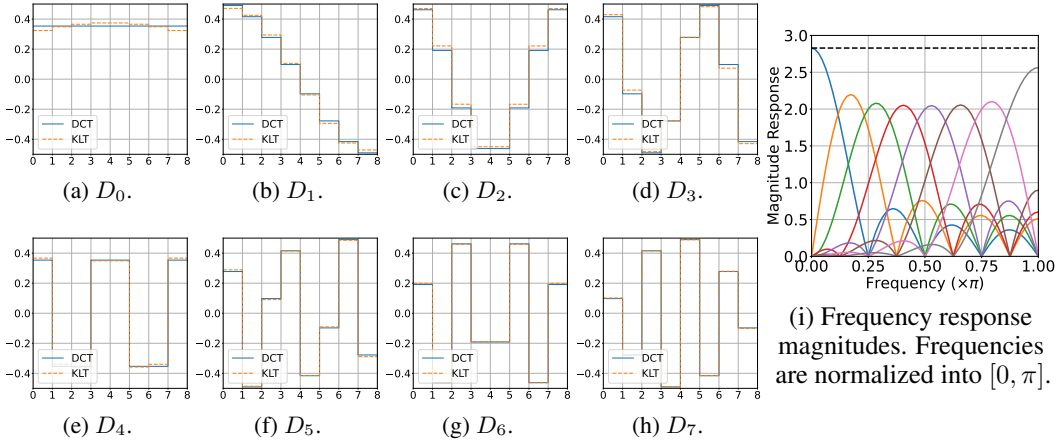


Figure 2: Basis vectors of an 8×8 DCT matrix and their frequency response magnitudes. D_i refers to the i -th column. The basis vectors provide a good approximation to the eigenvectors of the Teoplitz matrix with $\rho = 0.9$ (KLT). Each frequency response is shown in a solid curve in different colors, and their squared sum is denoted in the black dashed line, showing the entire spectrum is covered.

3.5 Motivation of the DCT-based Compression

The mechanism behind the DCT-based compression mimics the Karhunen-Loeve transform (KLT), which is also known as principal component analysis (PCA), a mathematical technique used for dimensionality reduction in signal processing [24, 61]. Neighboring image patches are highly correlated with each other. During training, the attention matrices are inter-correlated because they are obtained using similar gradient vectors. Therefore, they can be decorrelated and compressed using DCT. When the input data is highly correlated, the covariance matrix can be approximated by a Teoplitz matrix ϕ of $[1, \rho, \rho^2, \dots, \rho^{C-1}]$ with $\rho < 1$ close to 1 [2]. This is the covariance matrix of an autoregressive model random process AR(1) with the correlation coefficient ρ [22, 46]. Figure 2 shows that DCT basis vectors approximate the KLT of a first-order Markov process with high correlation among the neighboring samples [13, 38]. We observe that \mathbf{Q} , \mathbf{K} , and \mathbf{V} have parameters with high correlations among themselves. We can directly use DCT in data compression since its matrix approximates the corresponding KLT matrix [1],

Although KLT can also be utilized in data compression, it requires massive computation for the covariance matrices and the corresponding eigenvectors of \mathbf{X} . On the other hand, DCT is very successful in decorrelating the data without computing the covariance matrix and eigenvectors. As a consequence, it is also used in JPEG image [50, 52] and MPEG video [15] compression methods.

4 Experimental Results

We conduct experiments on the CIFAR-10 [25] and ImageNet-1K [12] classification tasks and COCO 2017 detection and segmentation tasks [28]. Swin Transformers [29] are employed as the backbone network. Implementation details are presented in the technical appendices.

4.1 CIFAR-10 Classification

Training vision transformers from scratch on the CIFAR-10 dataset is notoriously difficult. We demonstrate the benefits of using our DCT initialization and DCT compression for the Swin Transformer Tiny (Swin-T) on from-scratch CIFAR-10 training to show the effectiveness of our methods on the small-scale dataset. Table 2 presents the performance comparison on the CIFAR-10 test dataset, where the number of parameters only counts trainable parameters.

We start by training Swin-T with the vanilla attention function for the baseline and obtain 90.51% accuracy on the CIFAR-10 test dataset. Then, we investigate the DCT-initialized attention in Swin-T on the CIFAR-10 datasets. The accuracy of Swin-T on the CIFAR-10 dataset is always improved regardless of which attention weight is initialized as the DCT matrix. When the weights to compute keys (\mathbf{K}) are initialized as the DCT matrices, the accuracy is improved to 90.83%.

Table 2: CIFAR-10 test dataset evaluation. In column ‘‘DCT’’, Q/K/V denotes the weights initialized as the DCT matrix, and numbers mean the proportion of coefficients kept in DCT-compressed attention. Models with higher or lower accuracy are highlighted in pink or cyan, respectively.

Model	DCT	Params (M)	Top-1 Acc.
Swin-T	-	27.53	90.51%
Swin-T	Q	27.53	90.78%
Swin-T	K	27.53	90.83%
Swin-T	V	27.53	90.81%
Swin-T	0.25	21.45	90.46%
Swin-T	0.5	22.67	90.67%
Swin-T	0.75	24.69	90.90%

Next, we evaluate the DCT-compressed attention with different truncating rates in Swin-T on the CIFAR-10 dataset. Table 2 presents when we only keep 25% of DCT coefficients, the number of trainable parameters is reduced from 27.53M to 21.45M (22.1% off), while the accuracy only drops 0.05%. If we keep more DCT coefficients, the accuracy even improves. If we keep 75% of DCT coefficients, the accuracy increases from 90.51% to 90.90%. This is because although the number of trainable parameters is reduced, transforming the input data into the frequency domain using DCT can boost the extraction of important features. As a result, fewer trainable parameters are required.

4.2 ImageNet-1K Classification

Table 3 presents the performance comparison on the ImageNet-1K dataset, where the number of parameters only counts trainable parameters. First, we investigate the DCT-initialized attention in the Swin-T and the Swin-S on the ImageNet-1K dataset. The accuracy on the ImageNet-1K validation dataset is always improved nevertheless which weight matrix is initialized as the DCT matrix. For example, when we initialize the weights to compute keys (K) as the DCT weights, the accuracy of Swin-T from 81.474% to 81.728% and Swin-S are improved from 83.196% to 83.378%, respectively.

Then, we evaluate the DCT-compressed attention with different truncating rates and compare the results with DCFormer [26], as it is also a DCT-based method to reduce the computational cost. Table 3 presents that when we keep 75% of DCT coefficients, we can obtain a comparable accuracy result on Swin-T and a slightly better accuracy result on Swin-S. Contrarily, the trainable parameters of the Swin-T and the Swin-S are reduced from 28.29M to 25.45M (13.1% off) and from 49.61M to 44.45M (10.4% off), respectively. Flops are reduced from 4.49G to 4.18G (6.9% off) and 8.13G to 8.74G (7.0% off), respectively. If fewer DCT coefficients are kept, the swim transformers can get further savings on parameters and computational overhead. Meanwhile, the accuracy will drop correspondingly. As a comparison, although DCFormer-SW-T/S [26] with $\tau = 2$ reduce the FLOPs significantly ($\tau = 2$ means $4\times$ frequency compression), the performance drops seriously because the DCFormer takes both low-pass and high-pass DCT components equivalent important.

We further evaluate the two proposed DCT-based attentions in the ViT-B-32 backbone [14] to verify their performance on other vision transformers. When we initialize the weights to compute keys (K) as the DCT weights, the accuracy of ViT-B-32 is improved from 73.120% to 73.614%. When we apply DCT-compressed attention with 75% coefficients kept, the accuracy increases from 73.120% to 73.226% while the number of trainable parameters and FLOPs decline from 88.22M to 75.83M (14.0% off) and reduced from 4.41G to 4.05G (8.2% off), respectively.

4.3 Ablation Study

Multiple DCT Initialization Table 4 presents the ablation study about initializing multiple matrices of \mathbf{W}_Q , \mathbf{W}_K , and \mathbf{W}_V as the DCT matrix. Although such an initialization still improves the accuracy for Swin-T and Swin-S, the improvement is smaller than with the single DCT initialization. For example, in the Swin-T experiments, if \mathbf{W}_Q and \mathbf{W}_K are both initialized as the DCT matrix, the top-1 accuracy is 81.540%, lower than 81.568% from initializing \mathbf{W}_Q only and 81.728% from initializing \mathbf{W}_K only. This deterioration is caused by the weight symmetry problem [20] from initializing the multiple weights as the same values. In other words, the attention mechanism is designed to attend to relevant information in the input sequence. If Q, K, and V are the same, the model may not

Table 3: ImageNet-1K validation dataset evaluation. After DCT, Q/K/V denotes the weights initialized as the DCT matrix, and numbers mean the proportion of coefficients kept in DCT-compressed attention. Our models with higher or lower top-1 accuracy are highlighted in pink or cyan, respectively.

Method	Params (M)	Flops (G)	Top-1 Acc.	Top-5 Acc.
Swin-T (Torchvision) [29]	28.29	4.49	81.474%	95.776%
PoolFormer-S24 [55]	21	3.5	80.3%	-
DCFormer-SW-T ($\tau = 1$) [26]	28.29	4.5	81.2%	-
DCFormer-SW-T ($\tau = 2$) [26]	28.29	1.3	79.2%	-
gSwin-T [17]	22	3.6	81.715%	-
Swin-T-DCT-Q	28.29	4.49	81.568%	95.862%
Swin-T-DCT-K	28.29	4.49	81.728%	95.862%
Swin-T-DCT-V	28.29	4.49	81.528%	95.850%
Swin-T-DCT-0.25	22.21	3.24	79.580%	94.936%
Swin-T-DCT-0.5	23.43	3.64	80.762%	95.520%
Swin-T-DCT-0.75	25.45	4.18	81.474%	95.728%
Swin-S (Torchvision) [29]	49.61	8.74	83.196%	96.360%
PoolFormer-M36 [55]	56	8.8	82.1%	-
DCFormer-SW-S ($\tau = 1$) [26]	49.61	8.7	82.8%	-
DCFormer-SW-S ($\tau = 2$) [26]	49.61	2.7	80.9%	-
gSwin-S [17]	40	7.0	83.014%	-
Swin-S-DCT-Q	49.61	8.74	83.298%	96.298%
Swin-S-DCT-K	49.61	8.74	83.378%	96.398%
Swin-S-DCT-V	49.61	8.74	83.200%	96.364%
Swin-S-DCT-0.25	38.54	6.28	81.840%	95.704%
Swin-S-DCT-0.5	40.76	7.07	82.622%	96.036%
Swin-S-DCT-0.75	44.45	8.13	83.202%	96.388%
ViT-B-32 [14]	88.22	4.41	73.120%	90.306%
ViT-B-32-DCT-Q	88.22	4.41	73.278%	90.574%
ViT-B-32-DCT-K	88.22	4.41	73.614%	90.870%
ViT-B-32-DCT-V	88.22	4.41	73.306%	90.502%
ViT-B-32-DCT-0.5	66.97	3.51	72.948%	90.390%
ViT-B-32-DCT-0.75	75.83	4.05	73.226%	90.642%

Table 4: ImageNet-1K ablation study on multiple weights initialization as the DCT matrix.

Model	DCT	Top-1 Acc.	Top-5 Acc.
Swin-T	-	81.474%	95.776%
Swin-T-DCT	Q	81.568%	95.862%
Swin-T-DCT	K	81.728%	95.862%
Swin-T-DCT	V	81.528%	95.850%
Swin-T-DCT	QK	81.540%	95.754%
Swin-T-DCT	QV	81.548%	95.748%
Swin-T-DCT	KV	81.536%	95.770%
Swin-S	-	83.196%	96.360%
Swin-S-DCT	Q	83.298%	96.298%
Swin-S-DCT	K	83.378%	96.398%
Swin-S-DCT	QK	83.208%	96.378%

effectively capture the relationships between different positions in the input sequence. Moreover, one of the advantages of self-attention is its ability to model complex dependencies between different positions in the sequence. If \mathbf{W}_Q , \mathbf{W}_K , and \mathbf{W}_V are the same, the capacity of the model to capture diverse patterns will be limited, and the performance of the model will drop correspondingly.

Non-Trainable DCT Weights Initialization In this case, computing queries, keys, and values is equivalent to shifting the DCT representation of the input patterns. Table 5 shows we obtain comparable accuracy results as the baseline but use fewer trainable parameters on the CIFAR-10 dataset. It also shows on the ImageNet-1K dataset if we take non-trainable DCT weights to compute

Table 5: Ablation study on non-trainable DCT weights.

Model	DCT	CIFAR-10		ImageNet-1K		
		Params (M)	Top-1 Acc.	Params (M)	Top-1 Acc.	Top-5 Acc.
Swin-T	-	27.53	90.51%	28.29	81.474%	95.776%
Swin-T	Q	25.37	90.47%	26.13	81.214%	95.674%
Swin-T	K	25.37	90.64%	26.13	81.302%	95.788%
Swin-T	V	25.37	90.75%	26.13	80.486%	95.236%
Swin-T	QK	23.21	90.70%	23.98	80.608%	95.446%
Swin-T	QV	23.21	90.50%	23.98	80.234%	95.208%
Swin-T	KV	23.21	90.62%	23.98	80.228%	95.276%

Q or K, the top-1 accuracy drops insignificantly (less than 0.3%). It is worthwhile noting that in this work, the DCT is implemented by matrix multiplication. Hence, the computational overhead of using non-trainable DCT weights is the same as the vanilla attention. Still, the DCT with butterfly operation can further reduce this cost as we only need to apply DCT in each attention layer.

4.4 COCO 2017 Object Detection and Instance Segmentation

We further evaluate the proposed methods on COCO 2017 object detection and instance segmentation tasks [28]. We use the Swin Transformers with ImageNet-1K pre-trained weights as the backbone and the Cascade Mask R-CNN [6, 7] as the pipeline. Since initializing \mathbf{W}_K as the DCT matrix obtains the best accuracy results in the ImageNet-1K experiments, we use Swin-T-DCT-K and Swin-S-DCT-K to evaluate the DCT-based initialization. As Table 6 presents, both Swin-T-DCT-K and Swin-S-DCT-K obtain slightly better average precision (AP) results than the vanilla models in the two tasks. Swin-T-DCT-0.75 obtains comparable AP results as Swin-T with about 3M fewer parameters, and Swin-S-DCT-0.75 gets better AP results than Swin-S with about 5M fewer parameters.

Table 6: COCO results. Our methods with higher or lower AP^{Mask} are highlighted in pink or cyan.

Backbone	Params (M)	Object Detection			Instance Segmentation		
		AP^{Mask}	$AP_{0.5}^{\text{Mask}}$	$AP_{0.75}^{\text{Mask}}$	AP^{Mask}	$AP_{0.5}^{\text{Mask}}$	$AP_{0.75}^{\text{Mask}}$
Swin-T [29]	86	50.3	69.1	54.3	43.7	66.6	47.3
DCFormer-T [26]	86	43.5	62.6	47.4	38.0	59.3	40.7
Swin-T-DCT-K	86	50.4	69.2	54.3	43.9	66.6	47.6
Swin-T-DCT-0.75	83	50.0	69.1	53.9	43.7	66.8	47.6
Swin-S [29]	107	51.8	70.4	56.3	44.7	67.9	48.5
DCFormer-S [26]	107	46.6	64.9	50.4	40.5	62.2	43.7
Swin-S-DCT-K	107	52.4	70.8	57.3	45.1	68.3	49.1
Swin-S-DCT-0.75	102	52.1	70.6	57.0	45.0	68.0	48.8

5 Limitation

DCT in this work is implemented by matrix multiplication because the fast DCT is not officially supported in PyTorch. In the future, we will implement fast DCT to further simplify the computation.

6 Conclusion

In this work, we introduced two new methods using Discrete Cosine Transform (DCT) to decorrelate the input in the attention for vision transformers. First, we presented a novel DCT-based initialization approach to address the challenges associated with training attention weights. We demonstrated a significant improvement over traditional initialization, providing a robust foundation for the attention mechanism. Second, we formulated a DCT-based compression method that can effectively reduce the computational overhead by truncating high-frequency components. It resulted in smaller weight matrices with compromising considerable accuracy. We validated the efficacy of these breakthroughs, showcasing their potential to enhance the performance and efficiency of

Transformer models in the classification tasks. These contributions underscore the importance of thoughtful initialization strategies and compression techniques in advancing the capabilities of the Swin Transformer architectures.

References

- [1] Nasir Ahmed, T. Natarajan, and Kamisetty R Rao. Discrete cosine transform. *IEEE transactions on Computers*, 100(1):90–93, 1974.
- [2] Ali N Akansu and Mustafa U Torun. Toeplitz approximation to empirical correlation matrix of asset returns: A signal processing perspective. *IEEE Journal of Selected Topics in Signal Processing*, 6(4):319–326, 2012.
- [3] Daniel Bolya, Cheng-Yang Fu, Xiaoliang Dai, Peizhao Zhang, and Judy Hoffman. Hydra attention: Efficient attention with many heads. In *European Conference on Computer Vision*, pages 35–49. Springer, 2022.
- [4] Stevo Bozinovski. Reminder of the first paper on transfer learning in neural networks, 1976. *Informatica*, 44(3), 2020.
- [5] Tim-Oliver Buchholz and Florian Jug. Fourier image transformer. In *Proceedings of the IEEE/CVF Conference on Computer Vision and Pattern Recognition*, pages 1846–1854, 2022.
- [6] Zhaowei Cai and Nuno Vasconcelos. Cascade r-cnn: Delving into high quality object detection. In *Proceedings of the IEEE conference on computer vision and pattern recognition*, pages 6154–6162, 2018.
- [7] Zhaowei Cai and Nuno Vasconcelos. Cascade r-cnn: High quality object detection and instance segmentation. *IEEE transactions on pattern analysis and machine intelligence*, 43(5):1483–1498, 2019.
- [8] Nicolas Carion, Francisco Massa, Gabriel Synnaeve, Nicolas Usunier, Alexander Kirillov, and Sergey Zagoruyko. End-to-end object detection with transformers. In *European conference on computer vision*, pages 213–229. Springer, 2020.
- [9] Wen-Hsiung Chen, CH Smith, and Sam Fralick. A fast computational algorithm for the discrete cosine transform. *IEEE Transactions on communications*, 25(9):1004–1009, 1977.
- [10] Lu Chi, Borui Jiang, and Yadong Mu. Fast fourier convolution. *Advances in Neural Information Processing Systems*, 33:4479–4488, 2020.
- [11] Ekin D Cubuk, Barret Zoph, Dandelion Mane, Vijay Vasudevan, and Quoc V Le. Autoaugment: Learning augmentation policies from data. *arXiv preprint arXiv:1805.09501*, 2018.
- [12] Jia Deng, Wei Dong, Richard Socher, Li-Jia Li, Kai Li, and Li Fei-Fei. Imagenet: A large-scale hierarchical image database. In *2009 IEEE conference on computer vision and pattern recognition*, pages 248–255. Ieee, 2009.
- [13] R Dony et al. Karhunen-loeve transform. *The transform and data compression handbook*, 1(1-34):29, 2001.
- [14] Alexey Dosovitskiy, Lucas Beyer, Alexander Kolesnikov, Dirk Weissenborn, Xiaohua Zhai, Thomas Unterthiner, Mostafa Dehghani, Matthias Minderer, Georg Heigold, Sylvain Gelly, et al. An image is worth 16x16 words: Transformers for image recognition at scale. In *International Conference on Learning Representations*, 2020.
- [15] Touradj Ebrahimi and Caspar Horne. Mpeg-4 natural video coding—an overview. *Signal Processing: Image Communication*, 15(4-5):365–385, 2000.
- [16] Xavier Glorot and Yoshua Bengio. Understanding the difficulty of training deep feedforward neural networks. In *Proceedings of the thirteenth international conference on artificial intelligence and statistics*, pages 249–256. JMLR Workshop and Conference Proceedings, 2010.
- [17] Mocho Go and Hideyuki Tachibana. gswin: Gated mlp vision model with hierarchical structure of shifted window. In *ICASSP 2023-2023 IEEE International Conference on Acoustics, Speech and Signal Processing (ICASSP)*, pages 1–5. IEEE, 2023.
- [18] Kaiming He, Xiangyu Zhang, Shaoqing Ren, and Jian Sun. Delving deep into rectifiers: Surpassing human-level performance on imagenet classification. In *Proceedings of the IEEE international conference on computer vision*, pages 1026–1034, 2015.

- [19] Kaiming He, Xiangyu Zhang, Shaoqing Ren, and Jian Sun. Deep residual learning for image recognition. In *Proceedings of the IEEE conference on computer vision and pattern recognition*, pages 770–778, 2016.
- [20] Shell Xu Hu, Sergey Zagoruyko, and Nikos Komodakis. Exploring weight symmetry in deep neural networks. *Computer Vision and Image Understanding*, 187:102786, 2019.
- [21] Wei Hu, Lechao Xiao, and Jeffrey Pennington. Provable benefit of orthogonal initialization in optimizing deep linear networks. In *International Conference on Learning Representations*, 2019.
- [22] Michael Jachan, Gerald Matz, and Franz Hlawatsch. Time-frequency-autoregressive random processes: Modeling and fast parameter estimation. In *2003 IEEE International Conference on Acoustics, Speech, and Signal Processing, 2003. Proceedings.(ICASSP'03).*, volume 6, pages VI–125. IEEE, 2003.
- [23] Debesh Jha, Nikhil Kumar Tomar, Vanshali Sharma, and Ulas Bagci. Transnetr: Transformer-based residual network for polyp segmentation with multi-center out-of-distribution testing. In *Medical Imaging with Deep Learning*, 2023.
- [24] Xiaozhong Ji, Boyuan Jiang, Donghao Luo, Guangpin Tao, Wenqing Chu, Zhifeng Xie, Chengjie Wang, and Ying Tai. Colorformer: Image colorization via color memory assisted hybrid-attention transformer. In *European Conference on Computer Vision*, pages 20–36. Springer, 2022.
- [25] Alex Krizhevsky, Geoffrey Hinton, et al. Learning multiple layers of features from tiny images. 2009.
- [26] Xinyu Li, Yanyi Zhang, Jianbo Yuan, Hanlin Lu, and Yibo Zhu. Discrete cosin transformer: Image modeling from frequency domain. In *Proceedings of the IEEE/CVF Winter Conference on Applications of Computer Vision*, pages 5468–5478, 2023.
- [27] Jingyun Liang, Jiezhong Cao, Guolei Sun, Kai Zhang, Luc Van Gool, and Radu Timofte. Swinir: Image restoration using swin transformer. In *Proceedings of the IEEE/CVF international conference on computer vision*, pages 1833–1844, 2021.
- [28] Tsung-Yi Lin, Michael Maire, Serge Belongie, James Hays, Pietro Perona, Deva Ramanan, Piotr Dollár, and C Lawrence Zitnick. Microsoft coco: Common objects in context. In *Computer Vision—ECCV 2014: 13th European Conference, Zurich, Switzerland, September 6-12, 2014, Proceedings, Part V 13*, pages 740–755. Springer, 2014.
- [29] Ze Liu, Yutong Lin, Yue Cao, Han Hu, Yixuan Wei, Zheng Zhang, Stephen Lin, and Baining Guo. Swin transformer: Hierarchical vision transformer using shifted windows. In *Proceedings of the IEEE/CVF international conference on computer vision*, pages 10012–10022, 2021.
- [30] Ilya Loshchilov and Frank Hutter. Decoupled weight decay regularization. In *International Conference on Learning Representations*, 2018.
- [31] James Martens et al. Deep learning via hessian-free optimization. In *ICML*, volume 27, pages 735–742, 2010.
- [32] Sarfaraz Masood and Pravin Chandra. Training neural network with zero weight initialization. In *Proceedings of the CUBE International Information Technology Conference*, pages 235–239, 2012.
- [33] Sachin Mehta and Mohammad Rastegari. Mobilevit: Light-weight, general-purpose, and mobile-friendly vision transformer. In *International Conference on Learning Representations*, 2021.
- [34] Hongyi Pan, Diaa Badawi, and Ahmet Enis Cetin. Block walsh–hadamard transform-based binary layers in deep neural networks. *ACM Transactions on Embedded Computing Systems*, 21(6):1–25, 2022.
- [35] Hongyi Pan, Emadeldeen Hamdan, Xin Zhu, Salih Atici, and Ahmet Enis Cetin. Multichannel orthogonal transform-based perceptron layers for efficient resnets. *IEEE Transactions on Neural Networks and Learning Systems*, 2024.
- [36] Hongyi Pan, Xin Zhu, Salih Furkan Atici, and Ahmet Cetin. A hybrid quantum-classical approach based on the hadamard transform for the convolutional layer. In *International Conference on Machine Learning*, pages 26891–26903. PMLR, 2023.

- [37] Adam Paszke, Sam Gross, Francisco Massa, Adam Lerer, James Bradbury, Gregory Chanan, Trevor Killeen, Zeming Lin, Natalia Gimelshein, Luca Antiga, et al. Pytorch: An imperative style, high-performance deep learning library. *Advances in neural information processing systems*, 32, 2019.
- [38] Anabeth P Radünz, Fábio M Bayer, and Renato J Cintra. Low-complexity rounded klt approximation for image compression. *Journal of Real-Time Image Processing*, pages 1–11, 2022.
- [39] Mark Sandler, Andrew Howard, Menglong Zhu, Andrey Zhmoginov, and Liang-Chieh Chen. Mobilenetv2: Inverted residuals and linear bottlenecks. In *Proceedings of the IEEE conference on computer vision and pattern recognition*, pages 4510–4520, 2018.
- [40] Andrew M Saxe, James L McClelland, and Surya Ganguli. Exact solutions to the nonlinear dynamics of learning in deep linear neural networks. *arXiv preprint arXiv:1312.6120*, 2013.
- [41] Carmelo Scribano, Giorgia Franchini, Marco Prato, and Marko Bertogna. Dct-former: Efficient self-attention with discrete cosine transform. *Journal of Scientific Computing*, 94(3):67, 2023.
- [42] Zhuoran Shen, Mingyuan Zhang, Haiyu Zhao, Shuai Yi, and Hongsheng Li. Efficient attention: Attention with linear complexities. In *Proceedings of the IEEE/CVF winter conference on applications of computer vision*, pages 3531–3539, 2021.
- [43] Jiechong Song, Chong Mou, Shiqi Wang, Siwei Ma, and Jian Zhang. Optimization-inspired cross-attention transformer for compressive sensing. In *Proceedings of the IEEE/CVF Conference on Computer Vision and Pattern Recognition*, pages 6174–6184, 2023.
- [44] Vladislav Sovrasov. ptflops: a flops counting tool for neural networks in pytorch framework, 2018–2024.
- [45] Peize Sun, Rufeng Zhang, Yi Jiang, Tao Kong, Chenfeng Xu, Wei Zhan, Masayoshi Tomizuka, Lei Li, Zehuan Yuan, Changhu Wang, et al. Sparse r-cnn: End-to-end object detection with learnable proposals. In *Proceedings of the IEEE/CVF conference on computer vision and pattern recognition*, pages 14454–14463, 2021.
- [46] Matteo Testa and Enrico Magli. Compressive estimation and imaging based on autoregressive models. *IEEE Transactions on Image Processing*, 25(11):5077–5087, 2016.
- [47] Nikhil Kumar Tomar, Annie Shergill, Brandon Rieders, Ulas Bagci, and Debesh Jha. Transresunet: A transformer based resu-net for real-time colon polyp segmentation. In *2023 45th Annual International Conference of the IEEE Engineering in Medicine & Biology Society (EMBC)*, pages 1–4. IEEE, 2023.
- [48] Asher Trockman and J Zico Kolter. Mimetic initialization of self-attention layers. *arXiv preprint arXiv:2305.09828*, 2023.
- [49] Ashish Vaswani, Noam Shazeer, Niki Parmar, Jakob Uszkoreit, Llion Jones, Aidan N Gomez, Łukasz Kaiser, and Illia Polosukhin. Attention is all you need. *Advances in neural information processing systems*, 30, 2017.
- [50] Gregory K Wallace. The jpeg still picture compression standard. *Communications of the ACM*, 34(4):30–44, 1991.
- [51] Karl Weiss, Taghi M Khoshgoftaar, and DingDing Wang. A survey of transfer learning. *Journal of Big data*, 3(1):1–40, 2016.
- [52] Weidong Xiao, Nianbin Wan, Alan Hong, and Xiaoyan Chen. A fast jpeg image compression algorithm based on dct. In *2020 IEEE International Conference on Smart Cloud (SmartCloud)*, pages 106–110. IEEE, 2020.
- [53] Haoran Xu, Benjamin Van Durme, and Kenton Murray. Bert, mbert, or bibert? a study on contextualized embeddings for neural machine translation. In *Proceedings of the 2021 Conference on Empirical Methods in Natural Language Processing*, pages 6663–6675, 2021.
- [54] Dongjie Ye, Zhangkai Ni, Hanli Wang, Jian Zhang, Shiqi Wang, and Sam Kwong. Csformer: Bridging convolution and transformer for compressive sensing. *IEEE Transactions on Image Processing*, 2023.
- [55] Weihao Yu, Mi Luo, Pan Zhou, Chenyang Si, Yichen Zhou, Xinchao Wang, Jiashi Feng, and Shuicheng Yan. Metaformer is actually what you need for vision. In *Proceedings of the IEEE/CVF conference on computer vision and pattern recognition*, pages 10819–10829, 2022.

- [56] Sangdoon Yun, Dongyoon Han, Seong Joon Oh, Sanghyuk Chun, Junsuk Choe, and Youngjoon Yoo. Cutmix: Regularization strategy to train strong classifiers with localizable features. In *Proceedings of the IEEE/CVF international conference on computer vision*, pages 6023–6032, 2019.
- [57] Bowen Zhang, Shuyang Gu, Bo Zhang, Jianmin Bao, Dong Chen, Fang Wen, Yong Wang, and Baining Guo. Styleswin: Transformer-based gan for high-resolution image generation. In *Proceedings of the IEEE/CVF conference on computer vision and pattern recognition*, pages 11304–11314, 2022.
- [58] Hongyi Zhang, Moustapha Cisse, Yann N Dauphin, and David Lopez-Paz. mixup: Beyond empirical risk minimization. In *International Conference on Learning Representations*, 2018.
- [59] Zheyuan Zhang and Ulas Bagci. Dynamic linear transformer for 3d biomedical image segmentation. In *International Workshop on Machine Learning in Medical Imaging*, pages 171–180. Springer, 2022.
- [60] Jiawei Zhao, Florian Tobias Schaefer, and Anima Anandkumar. Zero initialization: Initializing neural networks with only zeros and ones. *Transactions on Machine Learning Research*, 2022.
- [61] Lin Zhao, Zihao Wu, Haixing Dai, Zhengliang Liu, Tuo Zhang, Dajiang Zhu, and Tianming Liu. Embedding human brain function via transformer. In *International Conference on Medical Image Computing and Computer-Assisted Intervention*, pages 366–375. Springer, 2022.
- [62] Ce Zheng, Xianpeng Liu, Guo-Jun Qi, and Chen Chen. Potter: Pooling attention transformer for efficient human mesh recovery. In *Proceedings of the IEEE/CVF Conference on Computer Vision and Pattern Recognition*, pages 1611–1620, 2023.
- [63] Zhun Zhong, Liang Zheng, Guoliang Kang, Shaozi Li, and Yi Yang. Random erasing data augmentation. In *Proceedings of the AAAI conference on artificial intelligence*, volume 34, pages 13001–13008, 2020.
- [64] Xin Zhu, Daoguang Yang, Hongyi Pan, Hamid Reza Karimi, Didem Ozevin, and Ahmet Enis Cetin. A novel asymmetrical autoencoder with a sparsifying discrete cosine stockwell transform layer for gearbox sensor data compression. *Engineering Applications of Artificial Intelligence*, 127:107322, 2024.

A Technical Appendices

A.1 Implementation Details

Models are trained on a server with 8 NVIDIA A100 80GB GPUs using Python with PyTorch. The code of this work will be released upon the paper’s acceptance.

A.1.1 Classification Tasks Implementation Details

Training models for the image classification tasks from scratch mostly follow the settings in [29]. We employ AdamW optimizer [30] for 300 epochs using a cosine decay learning rate scheduler and 20 epochs of linear warm-up. We set the batch size as 1024, the initial learning rate as 0.001, and the weight decay as 0.05. Data augmentation is performed as the following: The CIFAR-10 augmentation follows [19]. First, the training images are padded with 4 pixels. Then, they are randomly cropped to get 32 by 32. Finally, the images are randomly flipped horizontally. The images are normalized with the means of [0.4914, 0.4822, 0.4465] and the standard variations of [0.2023, 0.1994, 0.2010]. The ImageNet-1K augmentation follows PyTorch Torchvision’s GitHub repository [37]¹. As a start, images are resized to make the smaller edge of the image 232 for Swin-T and 246 for Swin-S. Next, they are cropped to 224 by 224 images and randomly flipped horizontally. Techniques such as Autoaugment [11], mixup [58], cutmix [56], and random erasing [63] are applied. Images are normalized with the means of [0.485, 0.456, 0.406] and the standard variations of [0.229, 0.224, 0.225]. During the training, the best models are stored based on the top-1 accuracy on the CIFAR-10 test dataset and the ImageNet-1K validation dataset.

Flops computation for the Swin Transformers and our revisions uses the function “flops” in the official implementation of [29]². To follow their work, the flops from the Softmax function are omitted.

Flops computation for the ViT-B-32 and our revisions uses the function “ptflops” in the official implementation of [44], with manually adding the flops from DCT.

A.1.2 COCO Detection and Segmentation Tasks Implementation Details

Training models for the COCO tasks follow the settings in [29]. Models start from ImageNet-1K pre-trained weights. We use AdamW optimizer [30] for 36 epochs with an initial learning rate of 0.0001, weight decay of 0.05, batch size of 16, $3\times$ schedule, and multi-scale training [8, 45].

¹<https://github.com/pytorch/vision/tree/release/2.0/references/classification>

²https://github.com/microsoft/Swin-Transformer/blob/main/models/swin_transformer.py